Theor Chem Acc (2007) 117:1093–1104
DOI 10.1007/s00214-006-0224-z

REGULAR ARTICLE

An integrated computational tool for the study of the optical properties of nanoscale devices: application to solar cells and molecular wires

Filippo De Angelis · Simona Fantacci · Antonio Sgamellotti

Received: 20 August 2006 / Accepted: 13 October 2006 / Published online: 5 January 2007

Abstract We present a combined computational strategy for the study of the optical properties of nanoscale systems, using a combination of codes and techniques based on Density Functional Theory (DFT) and its Time Dependent extension (TDDFT). In particular, we describe the use of Car–Parrinello molecular dynamics simulations for the study of nanoscale devices and show the integration of the obtained results with available quantum chemistry codes for the calculation of TDDFT excitation energies, including solvation effects by continuum solvation models. We review some prototypical applications of this integrated computational strategy, ranging from the interaction of dye sensitizers with TiO_2 nanoparticles, of interest in the field of dye-sensitized solar cells, to transition metal molecular wires exceeding 3 nm length.

Keywords Car–Parrinello · TDDFT · Excited states · Nanoscale devices · Solar cells · Molecular wires

1 Introduction

There is currently a great interest in the theoretical and computational simulation of nanoscale systems and devices. Indeed, while a large amount of experimental data have been collected on the response of matter at the nanometric scale, a comparable development in the understanding of these systems is still to be achieved. The major difficulty in the theoretical and computational comprehension of nanoscale devices resides in the complexity of the systems under investigation. In particular, the complex interatomic interactions underlying nanoscale devices call the use of accurate computational techniques, while the large dimensions of the systems to be studied substantially limit the accuracy of the theoretical and computational tools which can be exploited. Moreover, even theoretical and computational tools showing a reasonable compromise between the accuracy and the scaling of the computational cost with the number of atoms still have to tackle the inherent complexity of systems composed by several hundred (thousand) atoms, which usually show a large number of local geometrical minima.

The situation is even more severe if one considers not only ground state properties, such as geometries and charge distributions, but wishes also to provide a description of properties related to excited states, such as absorption and emission of light or non-linear optical properties. Indeed, the accurate prediction by computational methods of the optical properties of small to medium molecules still represents a challenge in theoretical chemistry.

The development of ground state theoretical tools rooted in the Density Functional Theory (DFT) had a tremendous impact in theoretical and computational chemistry and materials science. The accuracy reached by current exchange–correlation functionals, especially hybrid ones, including some amount of Hartree–Fock exchange, coupled to the reasonable scaling of the computational cost as the cube of the number of atoms (or number of basis set functions), the increasing computer power of off-the-shelf PCs and the availability of general–purpose quantum-chemistry packages has led to the routinary application of DFT to systems of medium

F. De Angelis (✉) · S. Fantacci · A. Sgamellotti
Istituto CNR di Scienze e Tecnologie Molecolari (ISTM-CNR), c/o Dipartimento di Chimica, Università di Perugia, I-06213 Perugia, Italy
e-mail: filippo@thch.unipg.it

(25–50 atoms) dimensions also by non-specialist of the field.

Moreover, the possibility of performing DFT-based molecular dynamics simulations, by means of the Car–Parrinello method [1], allows researchers not only to investigate the geometry and electronic structure of relatively complex systems but also to investigate the dynamics of chemical reactions [2–5], to include the effect of thermal motion on the investigated properties [6–9] and to optimize the geometry of extended systems characterized by several local minima of the potential energy surface [10,11].

The inclusion of solvation effects by means of continuum solvation models [12–17] has further enlarged the scope of DFT-based computer simulations aimed at a realistic simulation of the investigated properties. Indeed, inclusion of solvation effects is mandatory to provide a direct connection of the calculated properties with the corresponding experimental quantities [18,19], which are usually measured in condensed phase.

Concerning the calculation of excited state properties, the Time-Dependent extension of DFT (TDDFT) [20] has become the method of choice in most recent applications, due to the accuracy of this method coupled to its reasonable scaling with the number of atoms composing the investigated system. Indeed, TDDFT can be as accurate as correlated ab initio techniques for the description of excited states [21], still maintaining a computational cost comparable to a Configuration Interaction with Single excitations (CIS). TDDFT is still limited to deal with excited states having single-excitation character and some problems of current exchange–correlation functionals have been highlighted for long-range charge-transfer excitations [22] in which the starting and arriving orbitals of a given transition do not overlap significantly. Nevertheless, TDDFT is currently successfully applied to the study of biological systems containing transition metal centers [10,24]. For these systems, upon inclusion of solvation effects and thermal motion, TDDFT can yield excitation energies within 0.1–0.2 eV from experimental values [7,25,26].

In dealing with the optical properties of nanoscale systems, we devised a computational strategy based on a combination of different codes and techniques rooted in DFT and TDDFT. In particular, we use the CP method for geometry optimizations, performing alternating free and damped CP simulations in the search for global minimum structures. We then plug the optimized structures into available quantum chemistry packages for electronic structure analysis followed by TDDFT calculation of vertical excitation energies. In doing so, we include solvation effects by means of continuum solvation models.

In the following we describe the main aspects of the computational tools used in our strategy and review some computational results obtained in the field of dye sensitized solar cells and transition metal molecular wires. Most of the presented results have been obtained in collaboration with the experimental groups of M Grätzel and S. Bernhard (EPFL-Switzerland and Princeton University, USA, respectively), so that direct comparison of theoretical and experimental data is available.

2 Methodology overview

2.1 Car–Parrinello

The Car–Parrinello (CP) method [1] is a classical molecular dynamics scheme based on an interatomic potential derived on the fly from DFT. In most standard implementations, the CP method employs a plane-wave (PW) basis set, even though recent CP implementations in localized functions exists [27]. PWs do not depend on atomic positions and are free of basis-set superposition errors. Total energies and forces on the atoms can be calculated using computationally efficient Fast Fourier Transform (FFT) techniques. Finally, the basis set convergence depends only upon the number of PWs included in the expansion of the electron density which is controlled by a cutoff in the kinetic energy of the PWs. A disadvantage of PWs is their extremely slow convergence in describing core states. To deal with this difficulty, one usually employs pseudopotentials (PPs) to model the interaction of the valence electrons with the ionic core (nucleus + core electrons). When using conventional (so-called norm-conserving, NC) PPs, very large PW basis sets are needed to represent the contracted p orbitals of O, N, F, and the 3d orbitals of the transition metal block. Moreover, using a PW basis set the calculation of the non-local Hartree–Fock exchange is extremely computationally demanding, so that conventional CP codes usually implement only non-hybrid exchange–correlation functionals.

An approach that drastically reduces the PW cutoff was proposed by Vanderbilt [29], who introduced "ultrasoft" (US) PPs. The normalized charge density is written as the sum of two terms, a soft part represented in terms of smooth Kohn–Sham orbitals, and a hard part which is treated as an augmented charge:

$$n(\mathbf{r}) = \sum_i \left[|\phi_i(\mathbf{r})|^2 + \sum_{nm,I} Q^I_{nm}(\mathbf{r}) \left\langle \phi_i | \beta^I_n \right\rangle \left\langle \beta^I_m | \phi_i \right\rangle \right]$$

The functions Q^{I}_{nm} and $\beta^{\mathrm{I}}_{\mathrm{n}}$ are characteristic of the ultrasoft PP. Under these conditions the CP equations read: [30]

$$\mu\ddot{\phi}_i = -\frac{\delta E_{\mathrm{tot}}}{\delta \phi_i^*} + \sum_j \Lambda_{ij} S\phi_j,$$

$$\mathbf{F}_I = M_I\ddot{\mathbf{R}}_I = -\frac{\partial E_{\mathrm{tot}}}{\partial \mathbf{R}_I} + \sum_{ij} \Lambda_{ij} \left\langle \phi_i \left| \frac{\partial S}{\partial \mathbf{R}_I} \right| \phi_j \right\rangle$$

where the generalized orthonormality constraints have been incorporated by introducing the Lagrange multipliers Λ_{ij} and μ and M_I are the fictitious mass for the electronic degrees of freedom and the atomic masses, respectively. Once self-consistency at fixed nuclear position has been achieved, a proper choice of the parameter μ and of the integration time step allows us to observe the system while evolving in a dynamics very close to the Born–Oppenheimer surface. Moreover, inclusion of a friction (damping) term in the CP equations allows to optimize molecular and periodic structures.

Our benchmarks indicate that US calculations are at least 2–3 times less expensive than NC calculations of comparable accuracy. Moreover, the efficient parallel implementation of the CP code with Vanderbilt pseudopotentials [31] (CPV) allows us to explore the geometry (dynamics) of systems composed by up to (several) few hundred atoms [10,11]. Notably, CP optimized geometries are usually as accurate as those obtained by conventional quantum chemistry methods as we checked in several cases [32–34].

2.2 Electronic structure analysis and TDDFT calculations

For analysis of the electronic structure and calculations of vertical excitation energies by TDDFT we resort to available quantum chemistry codes, such as the Amsterdam Density Functional (ADF) [35–37] and the Gaussian03 (G03) [38] program packages. Solvation effects are described by the Conductor-like Polarizable Continuum Model (C-PCM) [14], where for TDDFT calculations we use its non-equilibrium version [39], as implemented in G03. We noticed that non-hybrid exchange–correlation functionals tend to underestimate the HOMO–LUMO gap and consequently the excitation energies in Ru(II) dyes [18], compared to hybrid functionals which are found to yield excitation energies in better agreement with experimental values [25,26,40]. We therefore used hybrid functionals for all our more recent applications. The most time-consuming computational step in the solution of the TDDFT equations is the diagonalization of the Ω coupling matrix, whose eigenvalues correspond to excitation energies while from its eigenvectors oscillator strengths can be calculated and their analysis in terms of single orbital excitations offers insight into the nature of the electronic transitions. The matrices involved in problems of practical interest are usually too large to be kept in memory (they have dimension $2{*}N_{\mathrm{occ}}{*}N_{\mathrm{virt}}$) and an iterative disk-based Davidson diagonalization needs to be used. The characterization of high-lying excited states in dense spectra of large systems, such as conduction band states, involves therefore calculation of several hundred excited states.

3 Computational studies on dye-sensitized solar cells

Dye-sensitized solar cells (DSSCs) are currently attracting widespread academic and commercial interest for the conversion of sunlight into electricity because of their low cost and high efficiency [41,42]. In these cells, the dyes and the mesoporous TiO_2 films or nanoparticles represent the key components to reach high power conversion efficiencies. It was the extraordinary performance of the *cis*-dithiocyanato bis(2,2′-bipyridine-4,4′-dicarboxylate)ruthenium(II) sensitizer (N3) attached to nanocrystalline TiO_2 films that brought a significant advance in DSSCs technology [43].

The general operating mechanism of DSSCs involves as fundamental steps the absorption of a photon from the dye adsorbed on the TiO_2 surface, followed by efficient transfer of one electron onto the TiO_2 conduction band. To achieve high electron transfer quantum yields the dye needs to be strongly electronically coupled to the semiconductor and to absorb a broad range of visible light, producing long-lived excited states with energies almost matching those of TiO_2 conduction band.

Theoretical calculations can be of great help in the design of new solar cells sensitizers with improved characteristics [18,25,26,40,44–49]. In this respect we and others performed several investigations on N3 and on related complexes [18,25,26,40,44–49], providing a deep understanding of the character of the excited states involved in the absorption process [18], the effect of solvation [18] and pH on the electronic structure and absorption spectra [40], the effect of replacing the thiocyanate by chloride ligands [25], the effect of protonation and counterions on the optical properties [26], the effect of functionalization of the bipyridine ligands [26,49] and the effect of cis-trans isomerism on the DSSC efficiency [48].

A further step towards the optimization of charge injection from the dye to TiO_2 involves effective modeling of the electronic structure and optical properties of TiO_2 surfaces or nanoparticles. Indeed, to check the

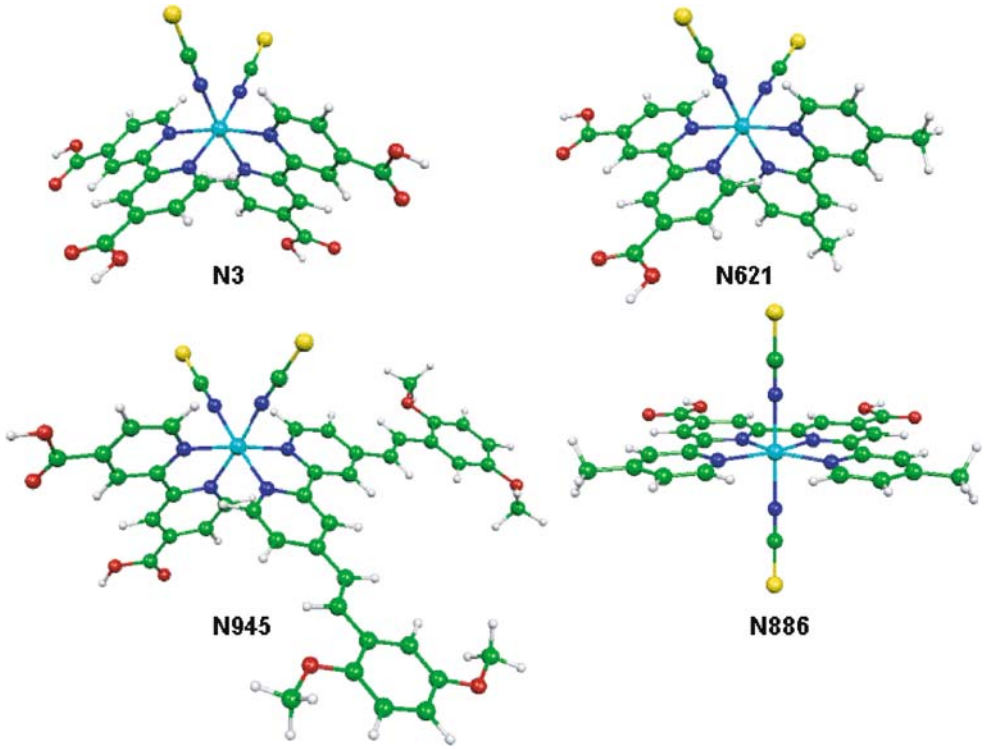

Fig. 1 Optimized molecular structures of some representative investigated Ru(II) dyes, labeled according to their conventional names. Light blue=Ru, yellow=S, red=O, blue=N, green=C and white=H atoms

viability of energetically favorable electron transfer pathways it is important to evaluate the alignment of the dye excited states (or more simply the dye LUMOs) with the semiconductor conduction band. In doing so one needs to migrate from the molecular scale to the nanoscale. In an effort in this direction we investigated a model of a TiO_2 nanoparticle of nanometric dimensions [50] and used this model to compare the energy levels of various dyes with the semiconductor band states [26]. Clearly, the ultimate goal in the theoretical simulation of DSSCs is the computational modeling of combined dye/semiconductor systems. As a first attempt in this direction we performed a study of the electronic structure and optical properties of $[Fe(CN)_6]^{4-}$ adsorbed on a TiO_2 nanoparticle [50], while a corresponding study of N3 adsorbed on TiO_2 is in progress. In the following we review our main computational results starting from the dye molecules, to TiO_2 nanoparticles, to the combined dye/TiO_2 systems.

3.1 Computational studies on solar cell sensitizers

We investigated by DFT/TDDFT calculations several Ru(II)–polypyridyl complexes, with the most representative ones being reported in Fig. 1. The most well-known Ru(II) sensitizer is the bis(2,2′-bipyridine-4,4′-dicarboxylate)ruthenium(II) complex (N3). Molecular engineering has then investigated chemical modifications of N3 to improve the light-harvesting capability of the complex, its thermal stability and ultimately its efficiency in DSSCs.

In Fig. 2 we report the comparison between the calculated and experimental absorption spectrum of the tetra-deprotonated N3 complex in water solution. For TDDFT calculations the B3LYP [51] functional and a DVZP basis set [52] has been used, including solvation effects by means of the non-equilibrium C-PCM. The geometry was in this case optimized in water solution with the B3LYP functional and a 3-21G* basis set [53]. The calculated spectrum has been obtained by convolution of the lowest 70 singlet–singlet TTDFT oscillator strengths centered on the calculated excitation energies. As it can be noticed, the agreement between theory and experiment both in terms of absolute energies, relative band intensities and overall spectral shape is excellent over an energy range of ca. 4.5 eV. Inspection of the TDDFT eigenvectors reveals that the two bands in the visible region, experimentally found at 2.51 and 3.37 eV and calculated at 2.59 and 3.41 eV, respectively, can be assigned as Metal to Ligand Charge Transfer excitations (MLCT), while the more intense band in the UV experimentally found at 4.03 eV and calculated at 4.18 eV is assigned as a bipyridine π–π^* transition. The MLCT bands originate from mixed Ru-NCS orbitals to

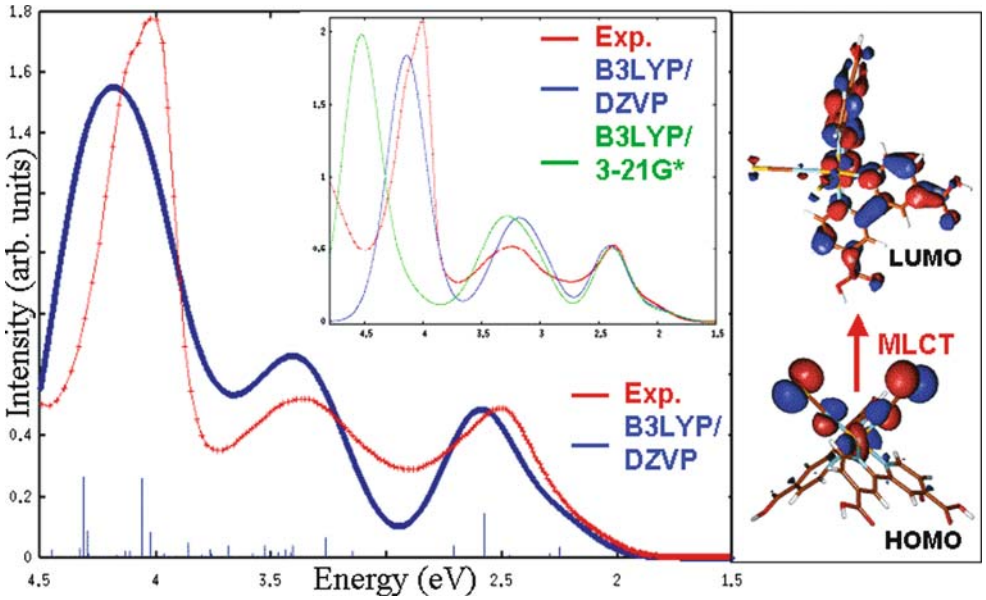

Fig. 2 Comparison between the experimental and calculated (B3LYP/DZVP) absorption spectrum of the tetradeprotonated N3 sensitizer. The inset shows a comparison between the experimental absorption spectrum of the related Cl complex, and the calculated spectra using the 3-21G* and DVZP basis sets. The intensity of the experimental spectra have been rescaled so as to match that of the calculated lowest MLCT band. Also shown are isodensity plots of the HOMO and LUMO of N3 contributing to the MLCT transitions

bipyridine π^* orbitals with sizable contributions from the bipyridine carboxylic groups, see Fig. 2. Since the dye adsorbs onto the TiO_2 surface by its terminal carboxylic groups, partial localization of the MLCT excited state at the dye-semiconductor interface assists charge injection. It is also interesting to investigate the effect of basis set on the calculated absorption spectra. We report in the inset of Fig. 2 a comparison between the experimental absorption spectrum of the related Cl complex, obtained by replacing the NCS by Cl ligands, and the calculated spectra using the 3-21G* and DVZP basis sets. As it can be noticed, while for the low-energy MLCT band the agreement between the two basis sets and the experiment is excellent, this agreement becomes progressively worse as the energy increases; this effect is particularly evident for the π–π^* transitions, which are considerably blue-shifted with the 3-21G* basis set.

3.2 Modeling TiO_2 nanoparticles

When modeling a TiO_2 nanoparticle it is mandatory to use a model large enough to show a well-developed band structure, so as to realistically mimic the electronic features of the real system. It is particularly important to reproduce the nanoparticle band gap and the energy of conduction band relative to that of the dye excited states. After several attempts with portions of TiO_2 anatase surfaces, we selected a $(TiO_2)_{38}$ cluster of nanometric dimensions [50] as our model, see Fig. 3. Periodic calculations as well as the final geometry optimization of the nanoparticle using a supercell approach have been performed with the CPV code, using the PBE functional [54]. The optimized geometry of the $(TiO_2)_{38}$ cluster was then used for calculation of the lowest TDDFT excitation energies, both in vacuo and in water solution. In doing so we used the B3LYP functional and the 3-21G* basis set, together with the non-equilibrium C-PCM. The 3-21G* basis represents a compromise between dimensions of the basis set and computational overhead and it allows a balanced description of the dye and of the nanoparticle. For the TiO_2 nanoparticle model the HOMO-LUMO gaps and lowest TDDFT excitation energies in vacuo and in solution are calculated to be 3.48 and 3.78 eV and 2.82 and 3.20 eV, respectively, the latter value being in excellent agreement with typical bandgaps of TiO_2 nanoparticles of a few nm size in solution [55,56]. On the one hand these results highlight the importance of solvation effects also for a correct description of the semiconductor electronic structure. On the other hand, the agreement between theory and experiment on the band gap makes us confident of the reliability of our model and level of theory.

Having a coherently correct description of the excited states of the Ru(II) dyes and of TiO_2 we used the data on the non-interacting species (B3LYP/3-21G*) to rationalize some interesting experimental trends in the efficiency of DSSCs. The overall conversion efficiency of the dye sensitized solar cell is determined by the prod-

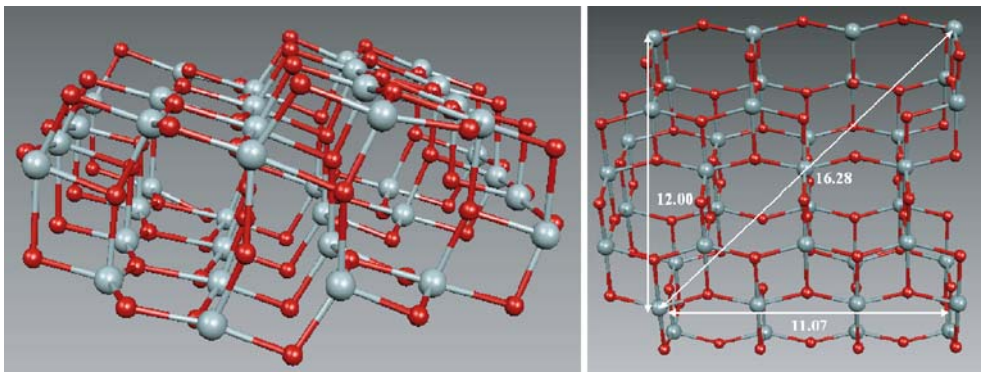

Fig. 3 Optimized molecular structure of the $(TiO_2)_{38}$ nanoparticle model. Main geometrical parameters (Å) are also reported. Red=O, grey=Ti atoms

uct of photocurrent density (i_{ph}), the open circuit potential (V_{oc}) and the fill factor (ff). The quantities amenable to a description at an atomistic level are the i_{ph}, which is related to coupling between the dye and semiconductor excited states, and V_{oc}, which is determined by the position of the quasi-Fermi level of the system, here assumed to be represented by the TiO_2 LUMO. Upon adsorption, the dye transfers most of its protons to the semiconductor, leading to an energy down-shift of the TiO_2 conduction band which in turn results in higher measured i_{ph}. This, however, reduces V_{oc} so that there should be an optimal degree of protonation of the sensitizer, for which the $i_{ph}V_{oc}$ product is maximized. Varying the degree of protonation of the sensitizer, however, introduces changes also in its electronic structure. We therefore investigated the various protonation states of N3 (from 4 to 0 protons) considering in each case the system with or without a corresponding number of Na^+ counterions. The results, in terms of a molecular orbital energy diagram and lowest singlet–singlet and singlet–triplet TDDFT excitation energies, are compared to those obtained for the bare TiO_2 nanoparticle in water solution in Fig. 4.

As it can be noticed, by decreasing the number of protons carried by the dye (moving from left to right of Fig. 4) the dye bipyridine π^* LUMOs are destabilized more than the Ru-NCS HOMOs, resulting in increased HOMO–LUMO gaps and lowest excitation energies. This LUMOs destabilization places the bipyridine π^* levels increasingly deeper into the TiO_2 conduction band.

Based on the present calculations, the di- and monoprotonated N3 species seem to represent an optimal choice with respect to the fully protonated and fully deprotonated species, since these dyes show a good light-harvesting capability coupled to an almost perfect alignment of their excited states with respect to the TiO_2 conduction band edge. Indeed, the fully protonated N3 species has an excellent light-harvesting capability, but the misalignment of the dye and TiO_2 LUMOs might imply that not all the absorbed light could be used for electron injection. The fully deprotonated species LUMOs, on the other hand, lie well above the TiO_2 conduction band edge, so that excited state relaxation to the bottom of the TiO_2 conduction band will involve some energy loss; also, the light-harvesting capability of this species in the low-energy spectral range is rather limited. Gratifyingly, despite the neglect of dye/semiconductor interactions in our mode, our theoretical observations are in line with experimental trends showing maximum efficiency for the di- and mono-protonated N3 dyes [26].

3.3 Dyes adsorption on TiO_2

A deep understanding of the dye/semiconductor coupling requires the explicit modeling of the combined system. In particular, a largely debated issue in the experimental community regards the mechanism of excited state charge injection from the dye to the semiconductor. For Ru(II)–polypyridyl dyes the generally accepted injection mechanism is an indirect one involving photoexcitation to a dye excited state, from which an electron is subsequently transferred to the semiconductor. By contrast, a mechanism involving a direct photoexcitation from the dye to an empty state of the nanoparticle is believed to occur for $[Fe(CN)_6]^{4-}$ on TiO_2. An indirect charge injection is generally signaled by an absorption spectrum of the dye/semiconductor system which is similar to that of the isolated dye in solution. On the other hand, a direct excitation should be characterized by the appearance of an absorption band at energies below the onset of the semiconductor band-to-band transitions. For the $[Fe(CN)_6]^{4-}/TiO_2$ system in acetonitrile or aqueous solution, a new band is effectively found in the absorption spectrum of the combined system at 2.95 eV (420 nm) [55]. In particular, we

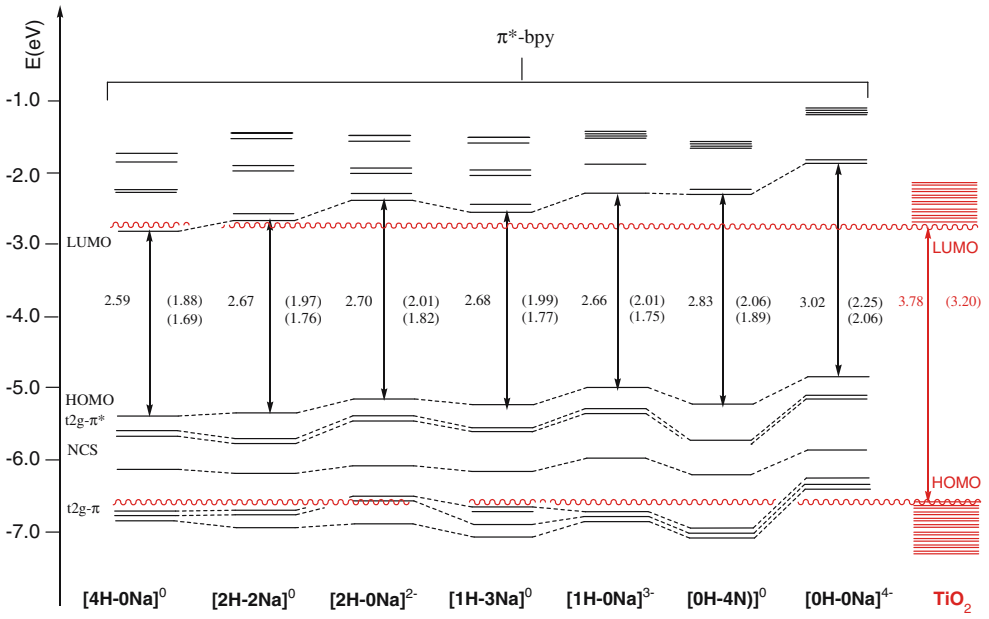

Fig. 4 Energy levels and lowest TDDFT excitation energies (data in parenthesis, first entry singlet-singlet, second entry singlet-triplet) calculated at the B3LYP/3-21G* level in water solution for the various species originated from the N3 dye, compared to results for the model TiO_2 nanoparticle. The edges of the TiO_2 valence and conduction band are represented as red discontinuous lines. We refer to the various N3-derived species as $[x\mathrm{H}-y\mathrm{Na}]^{(x+y-4)}$, where x is the number of protons, y is the number of sodium counterions and the total charge of the molecule is $(x+y-4)$

optimized the geometry of the combined $[Fe(CN)_6]^{4-}/TiO_2$ system, see Fig. 5a, by means of the CP method, followed by analysis of the electronic structure and TDDFT calculations in water solution (non-equilibrium C-PCM). In this stage we used the B3LYP functional, and 6-311G* and 3-21G* basis sets on $[Fe(CN)_6]^{4-}$ and TiO_2, respectively, for a total of 1972 basis functions. The large dimensions of the coupling matrix (770784) allowed us to calculate only the lowest 12 excitations, up to an energy of ca. 2.0 eV. Clearly, this energy range would not allow us to draw any conclusion concerning the appearance of the new band at ca. 3.0 eV. We therefore in this case complemented the TDDFT results by using a simplified approach in which excitation energies are approximated by Kohn–Sham orbital energy differences and oscillator strengths are obtained from dipole matrix elements between Kohn–Sham eigenstates [29]. Such an approximation was found to work quite well to describe the electronic excitations of large clusters and nanoparticles [35].

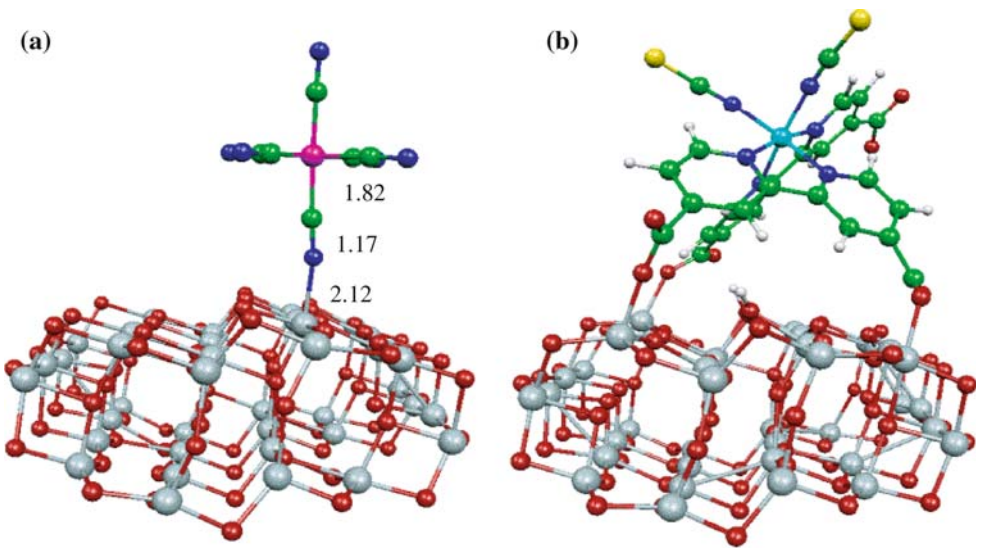

Fig. 5 Optimized geometrical structure of the $[Fe(CN)_6]^{4-}/TiO_2$ (a) and $N3/TiO_2$ (b) systems. Main bond distances (Å) for $[Fe(CN)_6]^{4-}/TiO_2$ are also reported. Grey=Ti, red=O, blue=N, green=C, purple=Fe, light blue=Ru, yellow=S, white=H

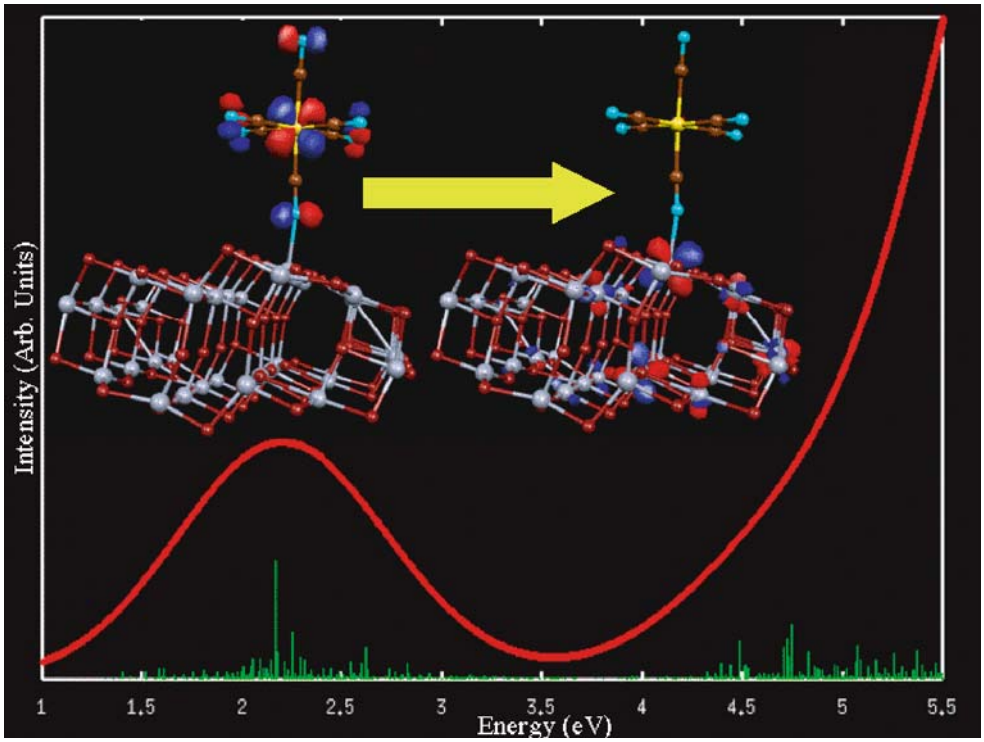

Fig. 6 Calculated optical absorption spectrum (eV) of $[Fe(CN)_6]^{4-}/TiO_2$. Isodensity plots of two of the orbitals involved in the transitions that maximally contribute to the intensity of the MPCT band are also shown

Electronic structure analysis revealed that the six HOMOs are essentially Fe t_{2g} and CN-based orbitals which lie within the TiO_2 band gap. The LUMOs are, on the other hand, a band of several TiO_2 conduction states which extend up to high energy. This electronic structure picture suggests already that the lowest excited states might be assigned as Metal to Particle Charge Transfer (MPCT) excitations. The lowest TDDFT excitation energy, calculated at 1.72 eV confirms the MPCT assignment based on the electronic structure. The overall absorption spectrum, reported in Fig. 6, exhibits a band at 2.75 eV, i.e. only 0.2 eV redshifted with respect to the experiment [55], and well below the onset of the nanoparticle interband transitions computed at ~4.3 eV. All the transitions composing this new low-energy feature are found to originate from the set of Fe t_{2g} dye HOMOs to unoccupied TiO_2 states, with no contributions from the lower set of CN-based dye levels nor from unoccupied dye states. Two of the orbitals involved in the series of most intense transitions composing this band are shown as insets in Fig. 6 and allow us to confirm the assignment of the low energy band as a MPCT transition and the direct injection mechanism.

We are currently extending our theoretical investigations to the $N3/TiO_2$ system. Preliminary results indicate that adsorption of the di-protonated dye is assisted by proton transfer from the dye to the TiO_2 surface, see Fig. 5b. Our optimized structure is rather different compared to that reported by Persson et al. for the tetraprotonated $N3/TiO_2$, system, which was adsorbed through two carboxylic groups of the same bipyridine ligand [59]. Further investigation on the coordination modes of the N3 dye on TiO_2 as a function of its protonation state and of its electronic structure and optical properties upon adsorption on TiO_2 are in progress.

4 Computational studies on ruthenium molecular wires

Molecular wires have become a topic of great interest in contemporary chemistry, physics and material science since they represent the fundamental component of nanoscale devices in molecular electronics [60,61]. These one-dimensional materials, which are characterized by a high electronic communication along the chains, can be used in many potential applications which range from TNT sensors to organic light emitting diodes [62,63]. A common structural feature of all molecular wires is that they are composed of monomeric subunits, which are concatenated to form oligomeric and polymeric systems. In an effort to engineer the properties of a molecular wire, it remains one of the foremost objectives to understand and control the factors

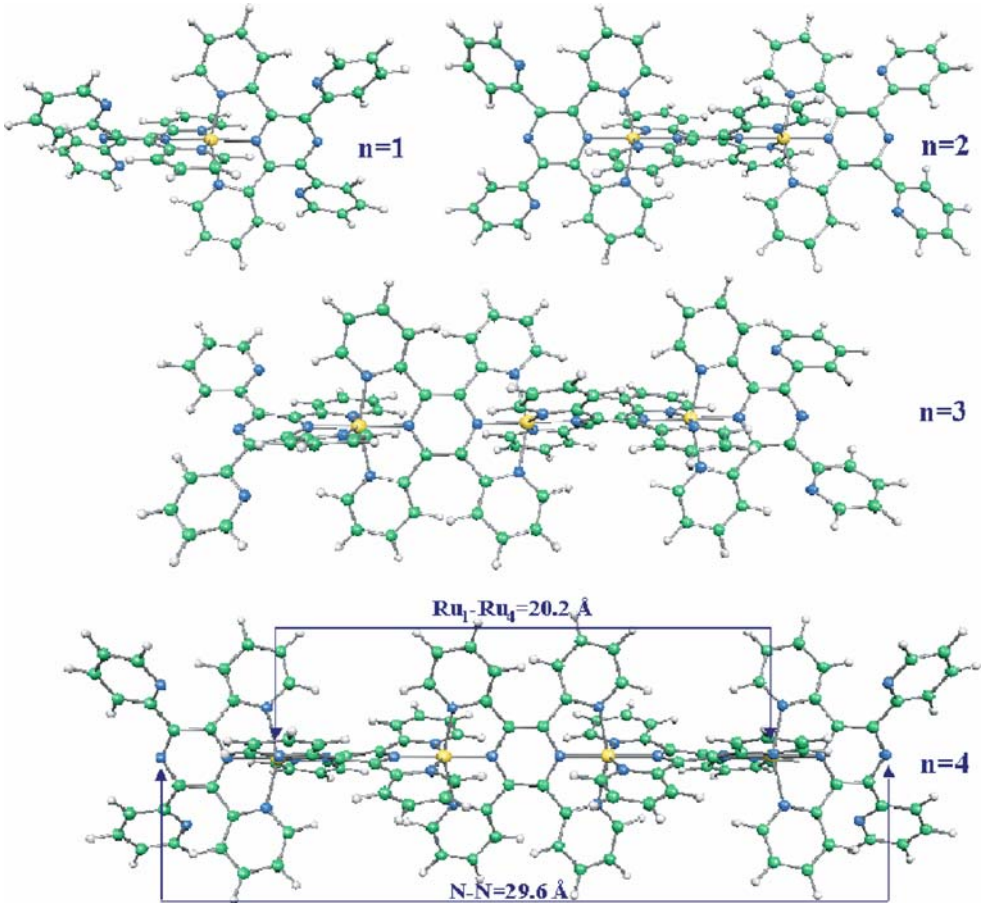

Fig. 7 Optimized molecular structures of the $[Ru_n(TPPZ)_{n+1}]^{2n+}$, TPPZ=tetra-2-pyridylpyrazine, complexes with n=1–4. For the n=4 species, main geometrical parameters (Å) are also reported. Blue=N, green=C, yellow=Ru, white=H

that influence the electronic communication among the building blocks and how the number of repeated units influences the molecular wire electronic structure. In this context we investigated a ruthenium(II) coordination polymer, of chemical formula $[Ru_n(TPPZ)_{n+1}]^{2n+}$, TPPZ=tetra-2-pyridylpyrazine, with interesting molecular wire properties [64]. In particular we carried out a full quantum mechanical investigation of the geometry, electronic structure and optical absorption spectra of the monomer and of the oligomers with n ranging from 1 to 4 using DFT and TDDFT calculations. We used the B3LYP functional together with LANL2DZ basis set [65–68] and pseudopotential [65–68] for Ru and the all-electron STO-3G minimal basis [69]. For the species with $n = 1$ and 2 we checked that the two basis sets yield consistently similar differences in the shift of the position and intensity of the visible absorption band, see below, going from $n = 1$ to 2 (0.42 vs. 0.37 with LANL2DZ and STO-3G, respectively), although the absolute value of the excitation energies are underestimated by ca. 0.25 eV using the minimal basis set. The molecular structures of the oligomers with $n = 1 - 4$, optimized by the CP method, are reported in Fig. 7. As it can be noticed, the larger $[Ru_n(TPPZ)_{n+1}]^{2n+}$ system, composed by 237 atoms, has exceeding nanometric dimensions (ca. 3 nm), implying the use of the smaller STO-3G basis.

The experimental absorption spectra of the investigated $[Ru_n(TPPZ)_{n+1}]^{2n+}$ complexes show a main absorption band in the visible region whose maximum shifts to lower energies as n is increased. Associated to this energy shift, an increase in the intensity of the main spectral feature is observed, with relative intensities (referred to that for the monomer spectrum) of 2.2 ($n = 2$) and 2.7 ($n = 3$). A comparison of the experimental spectrum of the monomer with that computed for the $[Ru(TPPZ)_2]^{2+}$ complex (B3LYP/STO-3G) in acetonitrile solution (non-equilibrium C-PCM) is presented in the inset of Fig. 8. The agreement between the two spectra is good, both in terms of band positions, relative intensity and overall spectral shape, especially considering the limited size of the basis set used for the calculations. The computed peak positions of the three bands agree within 0.1 eV with the experiment and only the

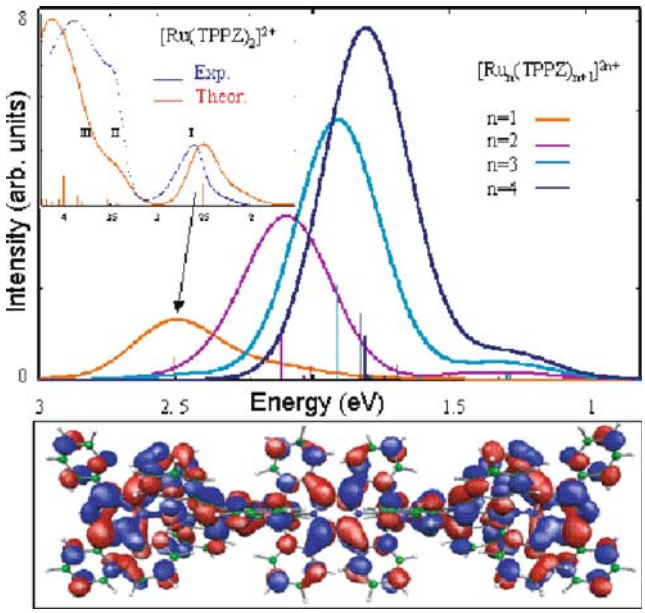

Fig. 8 Calculated absorption spectra in the visible region for the $[Ru_n(TPPZ)_{n+1}]^{2n+}$ complexes with n=1–4 in acetonitrile solution. The inset shows a comparison of the experimental and calculated absorption spectrum of the monomer in acetonitrile over a wider energy range. Also shown is a superposition of the tetramer orbitals involved in the intense visible transitions

relative intensity of the 3.4 eV shoulder is underestimated. The excited state giving rise to the intense transition in the visible at 2.51 eV has both Ru-t_{2g} and TPPZ-π^* character, delocalized over both the pyridyl and pyrazine ligands of the two TPPZ units, with sizable contributions of ruthenium d orbitals. We therefore assign band I as a metal to metal-plus-ligand charge transfer transition, whose intensity is related to the presence of metal orbitals in the final states as a consequence of π-back donation from the metal.

The computed spectra of the $n = 1 - 4$ oligomers in the visible region are shown in Fig. 8. The positions of the main absorption peaks agree well with the experiment, with a deviation of 0.27 eV at most, observed for the trimer. In particular, the observed red-shift and intensity increase of the main feature with increasing n are well described by the calculations. As for the monomer, also for $n > 1$ the most intense transitions in the visible show a sizable amount of metal character in the final states. The resulting excited states, being a superposition of Ru t_{2g}-TPPZ π^* states, are delocalized over the entire molecules, see Fig. 8, suggesting that the TPPZ units of the oligomeric species communicate through the intermediacy of the metal centers and of the central pyrazine bridges.

A property of considerable interest in the study of coordination polymers is the effective conjugation chain length (ECL) [70], associated to the extent of spatial conjugation in π-conjugated systems. In the investigated $[Ru_n(TPPZ)_{n+1}]^{2n+}$ complexes, the Ru octahedral coordination imposes an orthogonal arrangement of two consecutive TPPZ ligands bound to each metal center, so that an ECL restricted to a single or at most to a few TPPZ units might be expected. By plotting the theoretical and experimental peak energies, E_{max}, for the intense visible band as a function of the inverse number of TPPZ ligands, $1/(n + 1)$ it appears that, within the investigated range of TPPZ units, both computed and measured E_{max} show an approximately linear behavior. Both theoretical and experimental data show no saturation in the considered range of TTPZ units, implying that an ECL of several (> 6.5) TTPZ units is actually present in these Ru–TPPZ complexes. The origin of this remarkable effect is the extended charge delocalization in the excited states which is observed going from the monomer to the oligomers and is related to intermetal communication through the pyrazine bridges.

5 Conclusions

We have presented a computational strategy for the study of the optical properties of nanoscale systems. In particular, we have shown how one can integrate a combination of codes and techniques based on Density Functional Theory (DFT) and its Time Dependent extension (TDDFT) to provide detailed and accurate information concerning the ground and excited state properties of nanoscale devices. Particular emphasis has been posed on the description of the Car–Parrinello method, which allows us to perform DFT-based molecular dynamics simulations and geometry optimizations of complex systems. The inherent efficiency of the Car–Parrinello method implementing "ultrasoft" pseudopotentials and the available parallel implementation of the code allows us to optimize the geometry of extended systems composed by several hundred atoms, including up to several transition metal centers. We have then shown the integration of the obtained results with available quantum chemistry packages for the calculation of TDDFT excitation energies, including solvation effects by continuum solvation models, and we have reviewed prototypical applications of this integrated computational strategy, ranging from solar cells to molecular wires.

In the field of dye-sensitized solar cells (DSSCs) we have investigated the fundamental ingredients of the devices, i.e. the dye molecules and the TiO_2 nanoparticles, and eventually the joint dye/semiconductor systems. A description of the isolated dyes in solution allows

to draw accurate conclusions about the character of the dye excited states and to assist the design of new and more efficient solar cells sensitizers. A screening of the electronic and optical properties of dye sensitizers in relation to their use in DSSCs devices, however, requires explicit modeling of the semiconductor surfaces or nanoparticles. In this respect we have set up a TiO_2 nanoparticle model, composed by a $(TiO_2)_{38}$ cluster of nanometric dimensions, with optical properties in good agreement with experimental band gaps, and used this model to check the alignment of several dyes excited states with the edge of the TiO_2 conduction band. While this uncoupled model has shown to qualitatively account for the trends of efficiency exhibited experimentally in DSSCs devices, a detailed description of the dye/semiconductor coupling requires the explicit modeling of the combined system. In this context we have investigated the mechanism of excited state charge injection in $[Fe(CN)_6]^{4-}$ on TiO_2 and are currently investigating that of Ru(II)–polypyridyl dyes on TiO_2, for which direct and indirect charge injection processes, respectively, have been proposed on the basis of available experimental evidence. Our calculations performed on $[Fe(CN)_6]^{4-}/TiO_2$ confirm indeed a direct charge injection from a dye occupied orbital to an unoccupied TiO_2 state.

A field in which modeling of nanoscale devices is mandatory is that of molecular wires, which represent the fundamental component of nanoscale devices in molecular electronics. Indeed, to understand the factors that influence the electronic communication among the building blocks and how the number of repeated units influences the molecular wire electronic structure one needs to explicitly model systems of increasing size, up to the nanoscale. In this context we applied our computational strategy to the study of a ruthenium(II) coordination polymer, of chemical formula $[Ru_n(TPPZ)_{n+1}]^{2n+}$ with interesting molecular wire properties and carried out a full quantum mechanical investigation of the geometry, electronic structure and optical absorption spectra of the monomer and of the oligomers with n ranging from 1 to 4. The species with $n = 4$, composed by 237 atoms, has dimensions exceeding 3 nm length. The computed spectra of the $n = 1 - 4$ oligomers in the visible region agree well with the experiment, correctly reproducing the observed red-shift and intensity increase of the main feature with increasing n. Most notably, both theoretical and experimental data show no saturation effects with increasing n; this is due to the extended charge delocalization in the excited states observed going from the monomer to the oligomers, which is in turn related to intermetal communication through the pyrazine bridges.

We are finally extending the application of our computational strategy to the description of emission processes, such as fluorescence and phosphorescence [71], and to the study of the non-linear optical properties of extended systems [72,73].

Acknowledgments We thank A. Selloni for helpful discussions. This work was supported by MIUR (FIRB2003, "Molecular compounds and hybrid nanostructure materials with resonant and non resonant optical properties for photonic devices").

References

1. Car R, Parrinello M (1985) Phys Rev Lett 55:2471
2. De Angelis F, Fantacci S, Sgamellotti A (2006) Coord Chem Rev 250:1497
3. De Angelis F, Tarantelli F, Alunni S (2006) J Phys Chem B 110:11014
4. Andruniov T, Fantacci S, De Angelis F, Ferrè N, Olivucci M (2005) Angew Chem Int Ed 44:6077
5. Giannozzi P, De Angelis F, Marzari N (2005) Car R First principle molecular dynamics In: Yip S, (ed) Handbook of materials modeling Springer, Berlin Heidelberg New York
6. Pavone M, Cimino P, De Angelis F, Barone V (2006) J Am Chem Soc 128:4338
7. Crescenzi O, Pavone M, De Angelis F, Barone V (2005) J Phys Chem B 109:445
8. Pavone M, Benzi C, De Angelis F, Barone V (2004) Chem Phys Lett 395:120
9. Hetényi B, De Angelis F, Giannozzi P, Car R (2004) J Phys Chem 120:8632
10. Fantacci S, De Angelis F, Sgamellotti A, Marrone A, Re N (2005) J Am Chem Soc 127:14144
11. De Angelis F, Jarzecki A A, Car R, Spiro T G (2005) J Phys Chem B 109:3065
12. Miertus S, Scrocco E, Tomasi J (1981) Chem Phys 55:117
13. Barone V, Cossi M (1998) J Phys Chem A 102:1995
14. Cossi M, Rega N, Scalmani G, Barone V (2003) J Comput Chem 24:669
15. Klamt A, Schurmann G (1993) J Chem Soc Perkin 2 Trans 799
16. Klamt A, Jonas V (1996) J Chem Phys 105:9972
17. Pye C C, Ziegler T (1999) Theor Chem Acc101:396
18. Fantacci S, De Angelis F, Selloni A (2003) J Am Chem Soc 125:4381
19. Alunni S, De Angelis F, Ottavi L, Papavasileiou M, Trantelli F (2005) J Am Chem Soc 127:15151
20. Casida M (1995) Time dependent density functional response theory for molecules In: Chong DP (ed) Recent advances in density functional methods vol 1, World Scientific, Singapore, p 155
21. Fantacci S, Migani A, Olivucci M (2004) J Phys Chem A 108:1208
22. Dreuw A, Head-Gordon M (2004) J Am Chem Soc 126:4007
23. Tozer DJ; Amos RD, Handy NC, Roos BO, Serrano-Andres L (1999) Mol Phys 97:859
24. De Angelis F, Car R, Spiro TG (2003) J Am Chem Soc 125:15710
25. De Angelis F, Fantacci S, Selloni A, Nazeeruddin MK (2005) Chem Phys Lett 415:115
26. Nazeeruddin MK, De Angelis F, Fantacci S, Selloni A, Viscardi G, Liska P, Ito S, Takeru B, Grätzel M (2005) J Am Chem Soc 127:16835

27. Iyengar SS, Schegel HB, Millan JM, Voth GA, Scuseria GE, Frisch MJ (2001) J Chem Phys 114:9758
28. Schegel HB, Millan JM, Iyengar SS, Daniels AD, Scuseria GE, Frisch MJ (2001) J Chem Phys 115:10291
29. Vanderbilt D (1990) Phys Rev B 41:7892
30. Pasquarello A, Laasonen K, Car R, Lee C, Vanderbilt D (1992) Phys Rev Lett 69:1982
31. Giannozzi P, De Angelis F, Car R (2004) J Chem Phys 120:5903
32. Fantacci S, De Angelis F, Sgamellotti A, Re N (2004) Chem Phys Lett 396:43
33. De Angelis F, Sgamellotti A, Re N (2002) Organometallics 21:2715
34. Fantacci S, De Angelis F, Sgamellotti A, Re N (2001) Organometallics 20:4031
35. te Velde G, Bickelhaupt F M, Baerends EJ, van Gisbergen SJA, Fonseca-Guerra C, Snjders J G, Ziegler T (2001) J Comput Chem 22:931
36. te Velde G, Baerends EJ (1992) J Comp Phys 99:84
37. Baerends EJ, Ellis DE, Ros P (1973) Chem Phys 2:42
38. Frisch MJ, Trucks GW, Schlegel HB, Scuseria GE, Robb MA, Cheeseman JR, Montgomery Jr JA, Vreven T, Kudin KN, Burant JC, Millam JM, Iyengar SS, Tomasi J, Barone V, Mennucci B, Cossi M, Scalmani G, Rega N, Petersson GA, Nakatsuji H, Hada M, Ehara M, Toyota K, Fukuda R, Hasegawa J, Ishida M, Nakajima T, Honda Y, Kitao O, Nakai H, Klene M, Li X, Knox JE, Hratchian HP, Cross JB, Adamo C, Jaramillo J, Gomperts R, Stratmann RE, Yazyev O, Austin AJ, Cammi R, Pomelli C, Ochterski JW, Ayala PY, Morokuma K, Voth GA, Salvador P, Dannenberg JJ, Zakrzewski VG, Dapprich S, Daniels AD, Strain MC, Farkas O, Malick DK, Rabuck AD, Raghavachari K, Foresman JB, Ortiz JV, Cui Q, Baboul AG, Clifford S, Cioslowski J, Stefanov BB, Liu G, Liashenko A, Piskorz P, Komaromi I, Martin RL, Fox DJ, Keith T, Al-Laham MA, Peng CY, Nanayakkara A, Challacombe M, Gill PMW, Johnson B, Chen W, Wong MW, Gonzalez C, Pople JA (2003) Gaussian 03, Revision B.05. Gaussian, Inc., Pittsburgh PA
39. Cossi M, Barone V (2001) J Chem Phys 115:4708
40. De Angelis F, Fantacci S, Selloni A (2004) Chem Phys Lett 389:204
41. Grätzel M (2001) Nature 414:338
42. O'Regan B, Grätzel M (1991) Nature 53:737
43. Nazeeruddin M K, Kay A, Rodicio I, Humphry-Baker R, Muller E, Liska P, Vlachopoulos N, Grätzel M (1993) J Am Chem Soc 115:6382
44. Guillemoles J F, Barone, Joubert L, Adamo C (2002) J Phys Chem A 106:11354
45. Monat J E, Rodriguez J H, McCusker J K (2002) J Phys Chem 106:7399
46. Cecchet F, Gioacchini A M, Marcaccio M, Paolucci F, Roffia S, Alebbi M, Bignozzi C A (2002) J Phys Chem B 106:3926
47. Rensmo H, Södergren S, Patthey L, Westmark K, Vayssieres L, Khole O, Bru hwiler PA, Hagfeldt A, Siegbahn H (1997) Chem Phys Lett 274:51
48. Barolo C, Nazeeruddin M K, Fantacci S, Di Censo D, Compte P, Liska P, Viscardi G, Quagliotto P, De Angelis F, Grätzel M (2006) Inorg Chem 45:4642
49. Nazeeruddin M K, Bessho T, Ito S, Klein C, De Angelis F, Fantacci S, Comte P, Liska P, Imai H, Grätzel M (2006) J. Photochem Photobiol A (in press)
50. De Angelis F, Tilocca A, Selloni A (2004) J Am Chem Soc 126:15024
51. Becke A D (1993) Chem Phys 98:5648
52. Godbout N, Salahub D R, Andzelm J, Wimmer E (1992) Can J Chem 70:560
53. Binkley J S, Pople J A, Hehre W J (1980) J Am Chem Soc102:939
54. Perdew J P, Burke K, Ernzerhof M (1996) Phys Rev Lett 77:3865
55. Khoudiakov M, Parise A R, Brunschwig B S (2003) J Am Chem Soc 125:4637
56. Weng YX, Wang YQ, Asbury JB, Ghosh HN, Lian T (2000) J Phys Chem B 104:93
57. Williamson A J, Grossman J C, Hood R Q, Puzder A, Galli G (2002) Phys Rev Lett 89:196803
58. Matxain J M, Mercero J M, Fowler J E,Ugalde J M (2003) J Am Chem Soc 125:9494
59. Persson P, Lundqvist M J (2005) J Phys Chem B 109:11918
60. Tour J M (2000) Acc. Chem. Res. 33:791
61. Balzani V, Juris A, Venturi M, Campagna S, Serroni S (1996) Chem Rev 96:759
62. Swager T M (1998) Acc Chem Res 31:201
63. Malliaras GG, Scott JC (2000) The chemistry, physics and engineering of organic light-emitting diodes In: Hadziioannou G, van Hutten PF (eds) Semiconducting Polymers. Wiley–VCH, New York, Weinheim
64. Fantacci S, De Angelis F, Wang, J, Bernhard S, Selloni A(2004) J Am Chem Soc 126:9715
65. Dunning TH Jr., Hay PJ In: Modern theoretical chemistry, vol. 3. Schaefer HF III (ed) Plenum, New York, p 1–28
66. Hay PJ, Wadt W R (1985) J Chem Phys 82:270
67. Wadt WR, Hay PJ (1985) J Chem Phys 82:284
68. Hay PJ, Wadt WR (1985) J Chem Phys 82:299
69. Hehre WJ, Stewart RF, Pople JA (1969) J Chem Phys 51:2657
70. Tsuda A, Osuka A (2001) Science 293:79
71. De Angelis F, Fantacci S, Sgamellotti A, Cariati E, Ugo R, Ford P C (2006) Inorg Chem (in press)
72. Locatelli D, Quici S, Roberto D, De Angelis F (2005) Chem Comm 5404:
73. De Angelis F, Fantacci S, Sgamellotti A, Cariati F, Roberto D, Tessore F, Ugo R (2006) Dalton Trans 852